Laser Ablation Mass Removal versus Incident Power Density during Solid Sampling for Inductively Coupled Plasma Atomic Emission Spectroscopy

Mark A. Shannon,† Xianglei L. Mao, Alberto Fernandez,‡ Wing-Tat Chan,§ and Richard E. Russo*

Lawrence Berkeley National Laboratory, Berkeley, California 94720

For laser ablation solid sampling, the quantity of material ablated (removed) influences the sensitivity of chemical analysis. The mass removal rate depends strongly on the laser power density, which is the main controllable parameter for a given material and wavelength parameter using laser solid sampling for inductively coupled plasma atomic emission spectroscopy (ICP-AES). For a wide variety of materials, a decrease in the rate of change, or roll-off, in mass removed is observed with increasing incident laser power density. The roll-off results from a change in the efficiency of material removed by the laser beam, primarily due to shielding of the target from the incident laser energy by a laser–vapor plume interaction. Several analytical technologies were employed to study the quantity of mass removed versus laser power density. Data for mass ablation behavior versus laser power density are reported using ICP-AES, atomic emission from a laser-induced plasma near the sample surface, acoustic stress power in the target, and measurements of crater volumes. This research demonstrates that the change in ICP-AES intensity with laser power density is due to changes in the mass removal. The roll-off in mass ablation is not due to a change in particle size distribution of the ablated species, fractionation of the sample, or a change in transport efficiency to the ICP torch. Accurate tracking of the ICP-AES with the laser ablation process justifies the use of internal and external standardization.

With readily available high-power lasers, a number of laser technologies are emerging which depend on removing mass from a target, including laser solid sampling for chemical analysis and spectroscopy, pulsed-laser thin-film deposition, and laser machining and microfabrication. In each application, knowledge of the amount of mass removed as a function of laser energy, spot size, pulse width, and wavelength is essential for understanding and controlling the desired application. The laser power density (energy per unit area and time) at the surface of an opaque target is *the* controllable parameter for mass removal.

For analytical spectroscopy, laser ablation sampling is suitable for the direct chemical analysis of complex solid samples.[1] Laser ablation has been used for sample introduction into the inductively coupled plasma (ICP) for subsequent analysis by atomic emission spectroscopy (AES)[1-4] or mass spectrometry (MS).[5-7] Direct analysis of the luminous laser-induced vapor plume (plasma) by emission spectroscopy is also suitable for direct solid chemical analysis.[8-10] The attraction of laser sampling over other methods is that a very small amount of material can be selectively removed from a solid for analysis, dissolution procedures are eliminated, and personnel exposure to the sample is minimized. However, the efficacy of laser ablation solid sampling depends on complex laser–material interaction processes. The amount and composition of mass removed is affected by the laser's intensity, wavelength, and pulse length, as well as the geometric, optical, and thermophysical properties of the material and the surrounding medium.[1-4] The goal for sampling solids with lasers is to have the vaporized material composition quantitatively match that of the parent solid, without knowing a priori the laser conditions required for any unknown material. This goal is difficult to achieve, since in general, laser–material interactions are highly nonlinear, particularly with respect to laser intensity. Different methods have been developed to improve precision and accuracy of solid sampling with lasers by using internal standards related to the laser ablation process.[11-14]

The purpose of this paper is to investigate the influence of laser irradiance on the amount of mass removed from a sample target and analyzed by ICP-AES. ICP-AES is a powerful tool for studying the laser material interaction at atmospheric pressure

---

† Permanent address: Department of Mechanical Engineering, University of Illinois at Urbana–Champaign, Urbana, IL 61801.

‡ Permanent address: Escuela de Quimica, Universidad Central de Venezuela, P.O. Box 47102, Caracas 1020-A, Venezuela.

§ Permanent address: Department of Chemistry, University of Hong Kong, Pokfulam Road, Hong Kong.

(1) Russo, R. E. Laser Ablation. *Appl. Spectrosc.* **1995**, *49*, A14–A28.

(2) Moenke-Blankenburg, L. *Spectrochim. Acta Rev.* **1993**, *15* (1), 1–37.

(3) Darke, S. A.; Tyson, J. F. *J. Anal. At. Spectrom.* **1993**, *8*, 145–209.

(4) Chan, W. T.; Russo, R. E. *Spectrochim. Acta* **1991**, *46B* (11), 1471–1486.

(5) Arrowsmith, P. *Anal. Chem.* **1987**, *59*, 1437–1444.

(6) Denoyer, E. R.; Fredeen, J. K.; Hager, J. W. *Anal. Chem.* **1991**, *63*, 445–457.

(7) Huang, Y.; Shibata, Y.; Morita, M. *Anal. Chem.* **1993**, *65*, 2999–3003.

(8) Leis, F.; Sdorra, W.; Ko, J. B.; Niemax, K. *Mikrochim. Acta* **1989**, *2*, 185–199.

(9) Majidi, V.; Joseph, M. R. *Crit. Rev. Anal. Chem.* **1992**, *23* (3), 143–162.

(10) Autin, M.; Briand, A.; Mauchien, P.; Mermet, J. M. *Spectrochim. Acta* **1993**, *48B* (6/7), 851–862.

(11) Richner, P.; Borer, M. W.; Brushwyler, K. R.; Hieftje, G. M. *Appl. Spectrosc.* **1990**, *44* (8), 1290–1296.

(12) Chen, G.; Yeung, E. S. *Anal. Chem.* **1988**, *60*, 2258–2263.

(13) Quentmeier, A.; Sdorra, W.; Niemax, K. *Spectrochim. Acta* **1990**, *45B* (6), 537–546.

(14) Mermet, J. M.; Ivaldi, J. C. *J. Anal. At. Spectrom.* **1993**, *8*, 795–801.

and versus a number of parameters (laser conditions, material composition, and gas medium).[1,4] Understanding the relationship between mass ablated and the ICP-AES intensity will aid fundamental laser–material interaction research as well as facilitate chemical analysis using laser solid sampling into an ICP. An important concern for internal standardization with ICP-AES is whether changes in ICP spectral emission versus changes and fluctuations in laser power density are due to the laser ablation process or to sample transport.

For laser ablation sampling with ICP-AES, the efficiency of mass removal plateaus or decreases as laser power density increases above some value.[1,4] ICP-AES signal intensity (sensitivity) is highly dependent on incident laser power density (ϕ). The laser ϕ can be adjusted by changing the laser energy and laser beam spot size on the sample. The ICP intensity, I, normalized to incident laser beam area, A, is related to the mass flux from the surface of the target for a given laser energy, if I is proportional to mass. The measurement of I/A follows a power law dependence, $I/A = C\phi^n$. Above a certain power density level, the coefficient n decreases, indicating a reduction or roll-off in the amount of material removed per unit laser energy. Roll-off in I/A with ϕ has been measured to occur when sampling metals, oxides, glasses, and high-temperature superconducting compounds.[1,4,15,16] The roll-off in I has been observed when using nanosecond excimer lasers at 248 and 308 nm wavelengths, as well as with a picosecond Nd:YAG laser at 1064, 532, and 266 nm wavelengths. The roll-off also has been observed in all the noble gas atmospheres.

Mass ablation roll-off is a concern for laser sampling into the ICP: the analytical sensitivity and compositional accuracy are influenced by the power density. Different phenomena have been proposed to describe the mass ablation behavior, including laser–vapor interactions, particle size changes, preferential vaporization (or fractionation) of composite materials, and changes in the transport of ablated mass to the ICP torch. The laser–vapor interaction (including processes such as plasma screening and laser-supported detonation) reduces the quantity of ablated mass per unit of incident laser energy.[17-20] The magnitude of ICP-AES intensity is assumed to be directly related to the amount of ablated mass that reaches the torch. Thus, if the ablated mass declines, the ICP signal will proportionally decline. If the particle size distribution of the ablated mass changes as a function of incident laser power density, as has been reported for laser sampling[21] and laser deposition of thin films,[22] then the transport efficiency to the ICP may change. Additionally, the vaporization, dissociation, and excitation of the ablated species in the torch is also a function of particle size distribution, which can further change the ICP-AES signal magnitude.[23]

(15) Fernandez, A.; Mao, X. L.; Chan, W. T.; Shannon, M. A.; Russo, R. E. *Anal. Chem.* **1995**, *67*, 2444–2450.
(16) Russo, R. E.; Mao, X. L.; Chan, W. T.; Bryant, M. F.; Kinard, W. F. *J. Anal. Spectrom.* **1995**, *10*, 295–301.
(17) Phipps, C. R.; Dreyfus, R. W. In *Laser Ionization Mass Analysis*; Vertes, A., Gijbels, R., Adams, F., Eds.; Wiley and Sons: New York, 1993.
(18) Boulmer-Leborgne, C.; Hermann, J.; Dubreuil, B. *Plasma Sources Sci. Technol.* **2**, 1993, 219–226.
(19) Radziemski, L. J.; Cremers, D. A., Eds. *Laser Induced Plasmas and Applications*; Marcel Dekker Inc.: New York, 1989.
(20) Beverly, R. E.; Walters, C. T. *J. Appl. Phys.* **1976**, *47*, 3485–3495.
(21) Arrowsmith, P.; Hughes, S. K. *Appl. Spectrosc.* **1988**, *42*, 1231–1236.
(22) Harkness, S. D.; Singh, R. K. *J. Appl. Phys.* **1994**, *75*, 669–671.
(23) Cromwell, E. F.; Arrowsmith, P. *Anal. Chem.* **1995**, *67*, 131–138.

To accurately and efficiently use laser ablation for sample introduction, we need to understand the mechanisms responsible for the roll-off and confirm that it is not an artifact of the sampling process. To study this behavior, we used four independent measurement technologies to investigate laser ablation versus incident power density. First, the vapor from laser-ablated samples (conducting and high-bandgap materials), as a function of laser beam spot size and energy, is introduced into an ICP and studied using AES. Second, the intensity of atomic emission within the laser-induced plasma (LIP) at the sample surface is monitored simultaneously with the ICP-AES intensity. Third, the mass removed as measured from the volume of the laser-induced craters, is related to power density. Finally, a physical phenomenon which is unaffected by particle size distribution in the vapor is used. The technology involves monitoring mechanical stress power of the acoustic response in the target material during the laser–material interaction. For each of these technologies, a roll-off in signal level is observed to occur, with the deflection point occurring at the same laser irradiance, indicating a change in mass flux versus laser power density. These measurements confirm that ICP-AES intensity correctly responds to the laser material interaction. Therefore, these findings support using an internal (ratio of elements) or external (acoustic monitor, laser-induced plasma) standard to improve quantitative analysis.

EXPERIMENTAL SECTION

The experimental configuration shown in Figure 1a for introducing a laser-ablated sample into an ICP has been previously described.[1,4,15,16] Briefly, the sample (target) is held in a chamber in which Ar gas passes and carries the ablated vapor to the central channel of a standard ICP torch. A quartz ablation chamber is used to observe the spatial AES of the LIP using another monochromator with a photomultiplier tube detector. Therefore, the intensities of the AES from both the ICP and the LIP are monitored simultaneously.[15] ICP and LIP emissions are measured versus laser energy and spot size for Cu, brass (Cu and Zn alloy), Zn, Al, Al_2O_3, Zr, Zr_2O_3, Fe, Fe_2O_3, Ta, and Sn. Crater volumes are calculated on the basis of both measurements of cross-sectional area using a stylus profilometer and microscopic measurements.

For the ICP-AES and LIP experiments, a Questek Model 2860 excimer laser at $\lambda = 248$ nm with a 30 ns pulse length and a Continuum 601C Nd:YAG laser at $\lambda = 266$ nm with a 35 ps pulse length were used to ablate 1 mm thick × 2 cm diameter targets. The beams from both lasers were apertured to 6 mm diameter and focused to various spot sizes on the target using a single 200 mm focal length plano-convex quartz lens. Spot diameters varied from ~50 μm to 1.3 mm for the highest to lowest power density, respectively. For the laser conditions and material properties utilized in this work, measured crater diameters were generally slightly less than the calculated laser beam spot size. The energy was controlled with a Newport 935-10 UV-grade high-power variable attenuator and was measured for each pulse with a photodiode pick-off calibrated to a NIST traceable Molectron PD-104 pulsed laser power meter. The spot sizes were determined by measuring with a microscope the ablation patterns made at the plane of incidence on UV burn paper.

The effect of transport and fluid dynamics on the ICP-AES signal intensity is studied by significantly changing the ablation chamber volume and flow path to the ICP. For the standard ICP-AES experiments, a short (~35 cm) length of 6 mm i.d. tubing
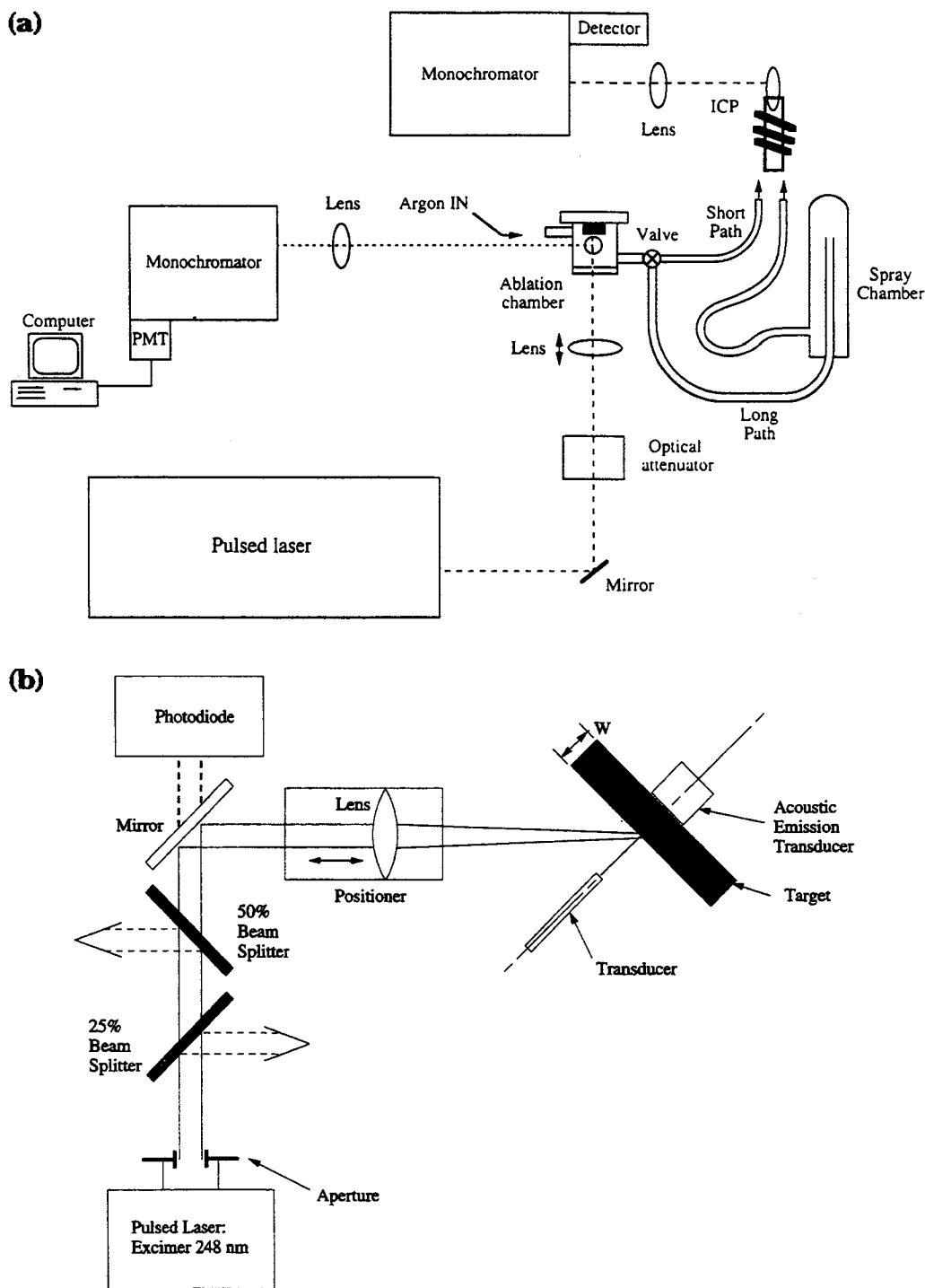
Figure 1. (a) ICP-AES and LIP-AES apparatus. CCD and photomultiplier tube detectors with monochromators for measuring ICP and LIP emission. Assembly to test transport effects: the short path consists of ~35 cm length of 6 mm i.d. tubing, and the long path is ~200 cm of tubing with a spray chamber to capture and condense particles. (b) Schematic of the stress power experimental system. Acoustic transducers record stresses transported through and above the target. Beam splitters are moved in and out for a total combination of four powers. Lens positioner changes spot size.

directly connected the ablation chamber to the ICP torch. To generate a convoluted path, a long (~200 cm) length of tubing connected the chamber to the torch, via a baffled spray chamber, as shown in Figure 1a. To compare the different paths, a weighted intensity is estimated by integrating over a sufficient time that the total ablated mass reaching the ICP torch is measured. The ratio I_{long}/I_{short} can be calculated to adjust the long path measurements with the same integration times as the short path.

The experimental setup for monitoring mechanical stress power of the acoustic emission is shown in Figure 1b. The laser

used is the Questek excimer. Power attenuation was achieved through a combination of 25% and 50% beam splitters and energy output adjustment of the excimer. The energy output ranged from 250 to 550 mJ/pulse. The excimer beam was passed through an 8 mm diameter aperture. The spot size was altered by translating the lens ($L_1 = 33$ mm at 248 nm) with respect to the target. A new location on the target was used for each energy level and spot size by shifting the target relative to the beam and transducers. The targets are 2 mm thick $\times$ 8 cm^2, 6061 Al in T6 condition, with both surfaces lapped flat to withint 10 μm/cm and finished
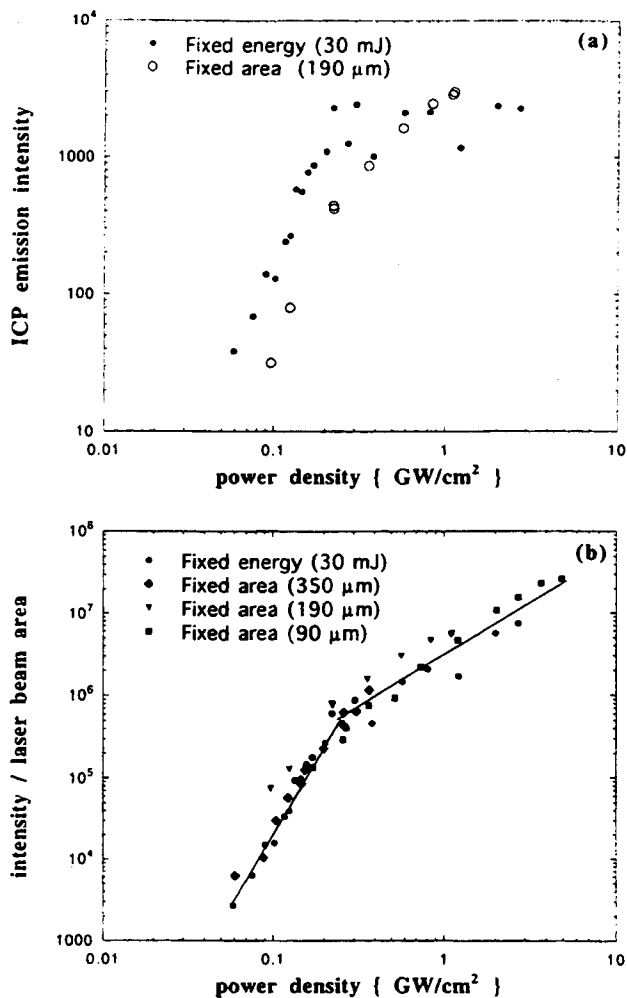
Figure 2. Laser ablation ICP-AES intensity of Cu at 327.4 nm. (a) Increasing laser energy at fixed spot size and fixed energy with reducing spot size. (b) ICP-AES intensity normalized to the area of the laser beam spot versus power density, showing the roll-off.

Figure 3. Laser power density at the measured roll-off point in the ICP emission intensity as a function of the melting temperatures of metals (●) and oxides (▲).

with 600 grit sandpaper. A 1 in. diameter acoustic emission transducer (AET) with a −3 dB frequency response from 10 kHz to 18 MHz was placed at the rear of the target, along the center line of the irradiated spot, to detect longitudinal and shear waves propagating through the material. A Valpey-Fisher Model VP-1093 0–1.2 MHz Pinducer was placed 5 mm from the surface along the center line normal to the spot to detect the density wave propagating through the air. All of the acoustic data were measured using a Tektronix Model 602A digitizing oscilloscope.

RESULTS AND DISCUSSION

1. **Inductively Coupled Plasma Atomic Emission Spectroscopy.** Using ICP-AES, a roll-off in mass ablation rate behavior versus laser power density is observed for a wide variety of materials, ambient gases, laser wavelengths, and laser pulse durations. In Figure 2, the ICP Cu emission line intensity at 327.4 nm is shown for laser ablation sampling of a copper target with the 30 ns excimer laser at 248 nm wavelength. The amount of material removed per laser shot is highly dependent on the laser irradiance, and roll-off is measured to occur for two cases: (i) when the laser energy is increased at fixed spot sizes and (ii) when the energy is constant and the spot size is reduced, as illustrated in Figure 2a. In Figure 2b, the ICP-AES intensity is normalized to the area of the laser beam spot and plotted versus
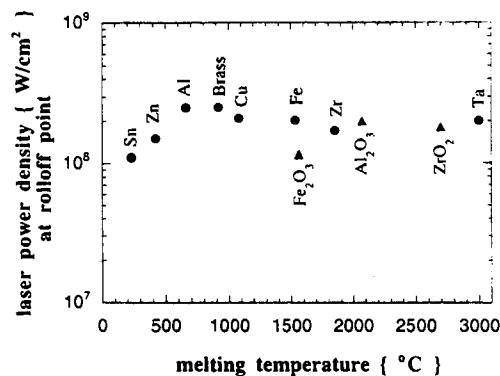
power density, spanning three different spot sizes. The normalized ICP-AES intensity increases with laser power density following a power law dependence of $I \propto \phi^n$. As shown in Figue 2b, when the power density is less than $\sim 3 \times 10^8 \, W/cm^2$, the power coefficient $n \approx 4$. At laser intensities above $3 \times 10^8 \, W/cm^2$, the intensity per unit area rolls-off to $n \approx 1$. In general, the coefficients for n vary between materials and ambient gas composition, target surface finish, and geometry, as well as with laser pulse width and wavelength. However, a superlinear dependence is always measured below $\sim 0.2 \, GW/cm^2$ for all materials investigated in this work (conductors and insulators), and the dependence decreases sharply above about $0.3 \, GW/cm^2$. The change in the slope indicates that a significant change in mass removal efficiency occurs before and after the roll-off point. The question is whether the mass removal roll-off is due to the laser−material interaction or is an artifact of laser sampling into an ICP (transport).

The roll-off of AES line intensity with power density is characteristic of laser sampling into the ICP for low, medium, and high melting point materials, ranging from 260 to 3000 °C. Moreover, the point of roll-off is relatively insensitive to material composition and target conditions. We measured the same roll-off behavior as in Figure 2 for nanosecond laser ablation sampling ICP-AES from targets of brass (Zn and Cu), Al, Al_2O_3, Fe, Fe_2O_3, Ta, Zn, Zr, ZrO_2, and Sn (some data shown in ref 1, 4, and 15). Roll-off behavior also has been reported for glass and high-temperature superconducting compounds.[16,24] The power density at roll-off versus each of the materials' melting temperatures is plotted in Figure 3 using emission intensities from the ICP. Regardless of the material's melting temperature, or whether the material was an insulator or a conductor, the laser power density at roll-off occurred between 0.1 and 0.3 GW/cm^2.

The weak dependence of melting temperature on the roll-off of mass removed with increasing laser power density is consistent with plasma shielding of a nanosecond pulsed laser beam. Plasma shielding of high-power nanosecond laser pulses occurs due to electron and thermionic emission from the laser target, inducing inverse-Brehmstraahlung (IB) absorption.[17] Since IB absorption grows exponentially in time with subnanosecond time scales, once the avalanche process has begun, material and atmosphere composition have a weak effect on plasma shielding. Therefore, once plasma shielding begins during nanosecond laser ablation, the melting temperature will have little effect. The threshold for

(24) Chan, W.-T.; Mao, X. L.; Russo, R. E. *Appl. Spectrosc.* **1992**, *46*, 1025–1031.
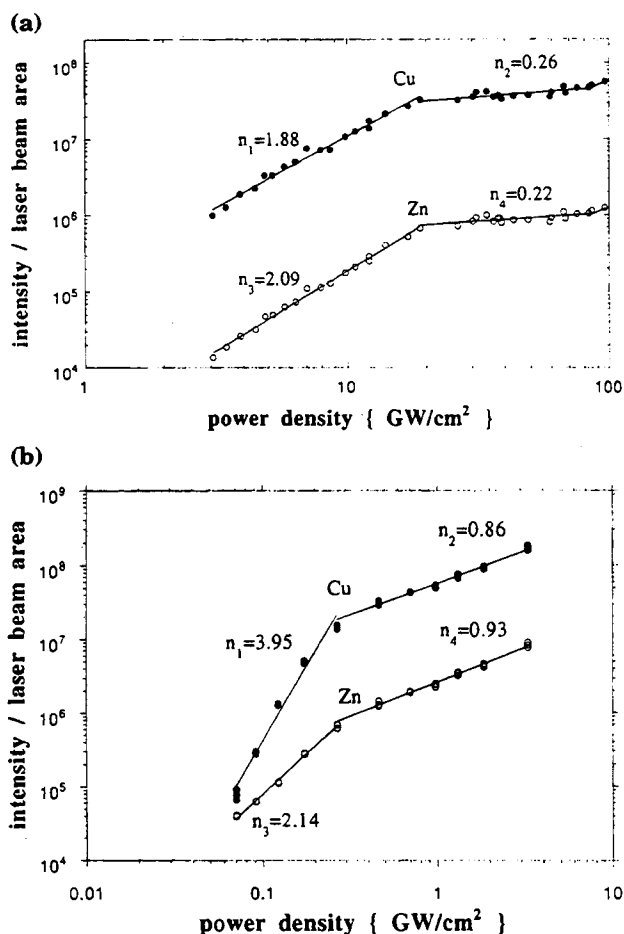
(a)

(b)

Figure 4. ICP-AES intensities of Cu and Zn from brass per unit laser area using (a) picosecond laser at 266 nm and (b) nanosecond laser at 248 nm. Graphs show roll-off of both Cu and Zn intensities for both lasers. For the nanosecond case, fractionation is occurring below the roll-off point of 0.3 GW/cm^2, as indicated by the different slopes. For the picosecond case, the Cu and Zn ratios remain constant.

nanosecond IB breakdown above solid targets in noble gases and N$_2$ has been estimated to be above 10^8 W/cm^2, which is consistent with the measured values in this work.[17] Other possible causes for the roll-off are time-dependent reflectivity and shock effects (laser-supported detonation),[19,20] which are worth further consideration. However, a study of fundamental mechanisms for laser—vapor interactions is outside the scope of this article on laser sampling for ICP-AES.

Roll-off in ICP-AES intensity has also been observed for picosecond UV ablation of a brass target, as illustrated in Figure 4a. The laser power density for the ICP intensity/area roll-off point is about 2 orders higher for pico- versus nanosecond ablation. Importantly, picosecond laser ablation sampling provides a higher ICP-AES intensity throughout the power density range, by about an order of magnitude compared to the nanosecond excimer laser.[25] In addition, the picosecond laser energy was only about 25% of that used for the nanosecond studies. Laser-supported detonation may be a possible contributor to the roll-off on the nanosecond time scale. However, laser-supported detonation is not likely possible on the picosecond time scale because the ablated vapor plume has only traveled a couple of micrometers

from the sample surface during the laser pulse. Plasma screening based on IB absorption with fast electrons and gas atoms has been proposed to describe the roll-off on the picosecond time scale.[25]

Particle Size Distribution. The insensitivity of roll-off for samples with widely varying melt temperatures (cf. Figure 3) provides important information about particle size distribution and transport. Particle ejection and particle size distribution scale with melting point for nanosecond and longer laser pulses due to melt ejection. At lower laser-induced sample temperatures, significant material is removed by melt ejection. Melt ejection decreases as the sample melting point increases.[26] If the roll-off in ICP-AES intensity is mainly due to particle ejection, the power density at roll-off would vary with melting point, but Figure 3 shows that the power density at roll-off is a weak function of melt temperature from 260 to 3000 °C. Also, particle size distribution varies between metals and oxides, since different mechanisms dominate for particle ejection (i.e., melt ejection versus fracture). However, little difference is seen between metals and their oxides. Since particle size distribution is a strong function of melting temperature and material composition, these data show that the roll-off cannot be due to changes in particle size distribution.

Fractionation. Another possible cause of roll-off in mass ablation for a particular element in a composite material could be preferential vaporization or fractionation.[1,4,23,24] In Figure 4b, relatively strong fractionation can be observed in the ICP-AES intensities during nanosecond excimer laser ablation sampling of brass in Ar as a function of power density, for both the copper and zinc atomic emission lines. Note that the coefficients for the copper lines ($n_1 = 3.95$, $n_2 = 0.86$) are similar to that for pure copper, as shown in Figure 2b ($n_1 = 4.03$, $n_2 = 1.15$), and the coefficients for the zinc lines are different ($n_3 = 2.14$, $n_4 = 0.93$). The mass of copper compared to zinc is not constant in the lower power density region before the roll-off; the composition of material ejected into the vapor phase is dependent on power density, leading to fractionation before, but not after, roll-off. Importantly though, the approximate roll-off point of (2–3) × 10^8 W/cm^2 is the same for both components. Fractionation, however, was not significant during UV picosecond laser ablation of brass, even though a roll-off in mass removal is observed. As seen in Figure 4a, the coefficients $n_1 \approx n_3$ and $n_2 \approx n_4$ for Cu and Zn. Therefore, roll-off in the mass removal rate with power density occurs with or without strong fractionation.

ICP Transport Issues. Another possible cause of roll-off in ICP-AES intensity with laser power density could be changes in the transport of the ablation products to the ICP torch. The causes of transport changes include variations in particle size distribution and thus transport efficiency, differing rates of vapor condensation on transport surfaces, and changes to the fluid dynamics caused by ablation pressure pulses. Each potential cause would be affected by changes in the length, volume, and convolution of the path from the ablation chamber to the ICP torch. An experiment was conducted to test transport issues by increasing the length of tubing from the ablation chamber and sending the vapor through a spray chamber (without any fluid) to alter the path, volume, and convolution of flow, as shown in Figure 1a. In Figure 5, the ICP-AES intensities for Cu are plotted versus laser power density for the short and long paths. Figure 5a shows the intensities between the two paths for the same integration time,

(25) Mao, X. L.; Chan, W. T.; Shannon, M. A.; Russo, R. E. *J. Appl. Phys.* **1993**, *74*, 4915–4922.

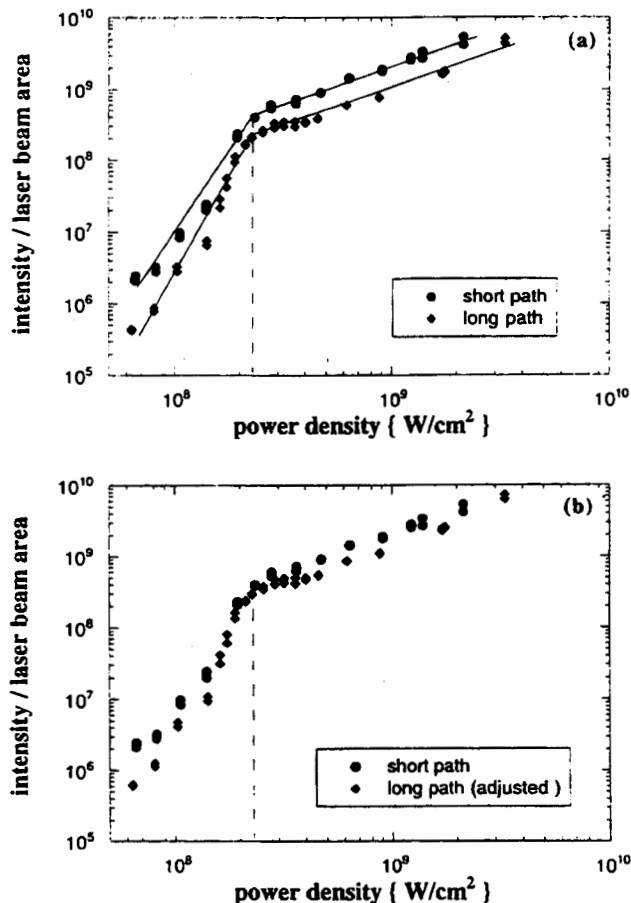(26) Ready, J. F. *Effects of High-Power Laser Radiation*; Academic Press: New York, 1971.

Figure 5. Roll-off in ICP-AES with different transport arrangements to the ICP, including both a short direct path and long tortuous path. (a) The same roll-off point for both paths, with only a difference in magnitude for identical sampling periods. (b) The long path intensity is adjusted for increased path length, which requires a longer integration time to capture all the ablated material that reaches the ICP torch.
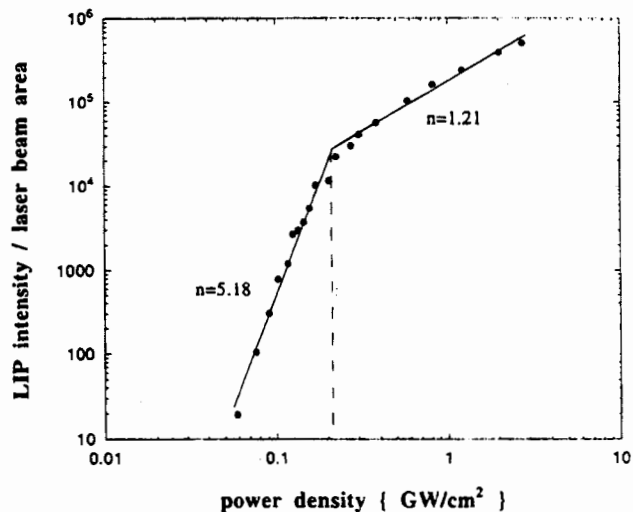

Figure 6. LIP-AES Cu line intensity at 521.8 nm, normalized to the area of the laser beam spot, plotted versus power density. Note similarities in roll-off with ICP-AES data shown in Figure 2.
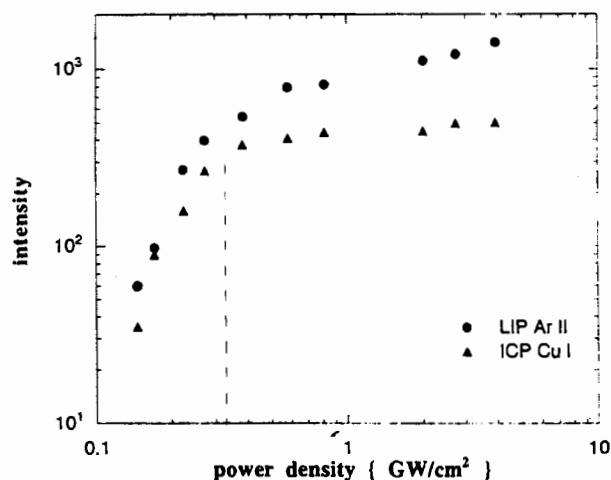

Figure 7. Simultaneously measured LIP-AES intensity for Ar II and ICP-AES intensity for Cu I plotted versus laser power density. Note that concurrent roll-off in both signals.

and Figure 5b gives the weighted intensities adjusted to give the total mass reaching the ICP torch. In both figures, the roll-off in ICP-AES intensities occurs at the same point. Moreover, the slopes are approximately the same as those in Figure 2b, and the weighted intensities are essentially collinear. Therefore, since these significantly different transport systems provide the same ICP-AES behavior, transport issues do not cause the roll-off.

2. Laser-Induced Plasma Atomic Emission Spectroscopy. To relate the ICP-AES emission intensity to the laser ablation process, the laser-induced plasma near the sample surface is monitored. The spectral emission intensity from the LIP is simultaneously recorded during ICP-AES measurements, as reported previously.[15] The LIP emission is a function of the number density of emitting species (which is related to the mass ablated) as well as the energy distribution of the total population (which is related to the excitation temperature). The exact relationship is a complicated function of the laser power, spot size, and material properties, as well as the expansion velocity of the plume and the integration time over which the LIP emission is measured.[27] However, the LIP emission is directly related to the mass of the high-energy vapor leaving the target surface.

Previously, a direct correlation of the LIP emission intensity with changes occurring in the ICP-AES was reported.[15] Laser-induced plasma emission shows a roll-off in intensity as a function of laser power density similar to that measured in the ICP, for both a change in energy and a change in the spot size, and for all the materials reported above. Figure 6 shows the LIP intensity at 521.8 nm from a copper target in an argon atmosphere with the 30 ns excimer laser at 248 nm wavelength for three different laser spot sizes and varying laser energy, normalized to spot area as a function of laser power density. The data in Figure 6 were simultaneously recorded with the ICP emission data shown in Figure 2b. These figures show that the roll-off in the ICP corresponds directly to the laser–material interaction recorded by the LIP.

An indirect measure of mass flux roll-off can be observed from the degree of ionization of the argon atmosphere above the target. Figure 7 shows that the Ar II emission intensity at 465.4 nm in the LIP rolls off at same power density as Cu emission intensity in the ICP, but with different slope. The Ar II intensity is observed over the entire plume expansion, which is orders of magnitude longer than the laser pulse; the ionized Ar is due to collisions
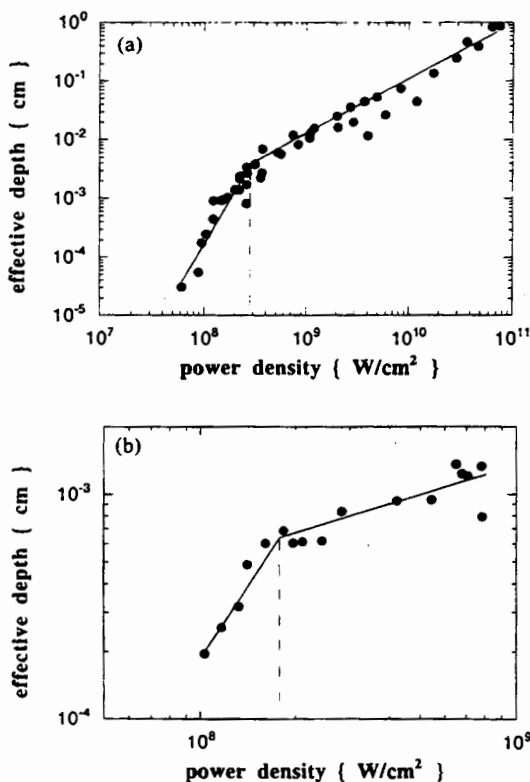
(27) Mao, X. L.; Shannon, M. A.; Fernandez, A. J.; Russo, R. E. *Appl. Spectroc.* **1995**, *49*, 1054–1062.

Figure 8. Measured crater volume/laser area versus power density for (a) Cu and (b) Fe. The average mass etch rate rolls off at the same power density as in the ICP and LIP data.

Figure 9. Roll-off of pressure pulse versus stress power in the target as a function of laser power density for Al. The roll-off power density is similar to that in the Al case for ICP and LIP. Each data point is per pulse and is not averaged. The pressure/stress ratio is directly related to mass removed.

between electrons, Cu, and Ar in the expanding plume. A direct increase in Ar II intensity due to absorbed laser light cannot be observed, since the integration time is longer than the pulse length. An increase in the measured Ar II intensity, however, is a result of increased numbers of high-energy collisions from ablated mass from the target. As laser power density increases, the mass flux leaving the surface increases, as does the temperature of the ablated species. The Ar II line intensity is a function of temperature and mass, and over the long expansion times measured, the temperature and mass flux are directly related. For these observations, as the laser power density increases, the average observed plume temperature for the full plume expansion at most slowly rises. Therefore, if the Ar II intensity is observed to roll off, then the mass flux must also be declining, but not necessarily at the same rate.

3. Mass Removal Observations. A direct measure of the mass removed is the volume of the craters formed after repetitive laser pulses. The volume of the craters was measured for a fixed number of laser pulses at each crater at each power density. Figure 8 shows the effective crater depth as a function of incident laser power density for Cu and Fe targets. The effective crater depth, defined as the measured crater volume divided by the laser beam area, is equivalent to the average mass removal rate. For both materials, the effective depth shows the same roll-off point as was determined with the ICP-AES and LIP-AES measurements. These crater measurements provide direct evidence for a change in mechanism. However, the crater data give an average mass removal rate over hundreds of pulses.

An acoustic monitoring method is used to obtain per pulse mass removal data for a nanosecond UV laser pulse. During high-power laser−material interactions, the vapor leaving the surface
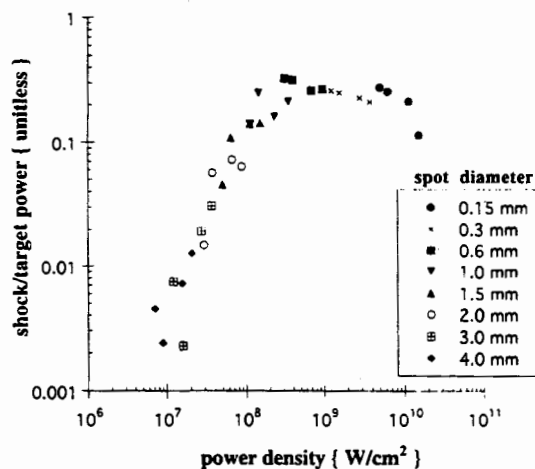
forms a shock wave, whose magnitude depends on the mass flux. Therefore, the magnitude of the pressure pulse will give a measure of momentum and the mass removed for a single laser pulse. The momentum recoil in the target may also be measured. The ratio of the pressure pulse leaving the target over the momentum recoil in the target depends on the amount of mass ablated. To monitor the ratio, acoustic emissions in the target and in the surrounding medium during each laser pulse are measured with stress transducers. The mechanical stress power in the transducers is subsequently calculated. The theory and development for using mechanical stress power is beyond the scope of this paper.[28] Basically, the stress power can be related to the momentum recoil of the mass being ablated from the surface. Figure 9 plots the rate of change in the ratio of the pressure pulse to the stress power in an Al target as a function of power density. At $\sim$0.2 GW/cm^2, the amount of laser energy coupled to the target has reached a plateau. Therefore, the amount of mass removed directly by the laser has ceased to increase with increasing laser energy. Heating by the laser-induced plasma, however, can further vaporize material from the target, albeit at a slower rate. Pérez and Weiner have used microbalances to directly measure mass removal per laser pulse.[29] Calculations we have made using their data for nanosecond laser ablation of gold thin films also show roll-off with power density at $\sim$0.3 GW/cm^2, as shown in Figure 10 (data from Table 1 in ref 29). Therefore, both average mass removal rates and mass removed per pulse show roll-off with laser power density at the same values as the ICP and LIP emission data.

CONCLUSION

The mass removed during high-power laser ablation depends nonlinearly on the incident laser power and spot size. Above a power density of $\sim$10^8 W/cm^2 for 30 ns and 10^{10} W/cm^2 for 35 ps laser pulses, the efficiency of the mass removed per unit of laser energy declines. The roll-off in mass removed occurs for a wide variety of materials with vastly different melting temperatures. These observations have important implications for using laser

(28) Shannon, M. A. Laser−materials interactions: A study of laser energy coupling with solids. Ph.D. Dissertation, University of California at Berkeley, 1993.

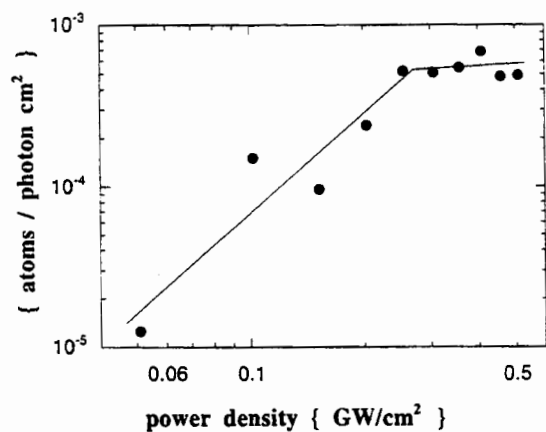(29) Pérez, J.; Weiner, B. R. *Appl. Surf. Sci.* **1992**, *62*, 281−285.

Figure 10. Photon efficiency for gold ablated by a 10 ns Nd:YAG laser at 532 nm, as measured by a microbalance (calculated from data in Table 1 of ref 29).

solid sampling with ICP-AES. Based on diverse experimental measurements, including monitoring the emission intensity from the laser-induced plasma, monitoring the stress power, crater volume measurements, and sample transport system changes, this research demonstrated that the behavior is due to changes in the laser–material interaction and not due to particle size distribution changes, fractionation, or transport changes in the ICP. The ICP accurately responds to variations in the laser–material interaction. Internal and external standardization technologies responding to the laser–material interaction can be employed to improve quantitative analysis using laser ablation sampling.